INTERNATIONAL JOURNAL OF HYDROGEN ENERGY XXX (2008) 1–12

Available at www.sciencedirect.com

ScienceDirect

journal homepage: www.elsevier.com/locate/he

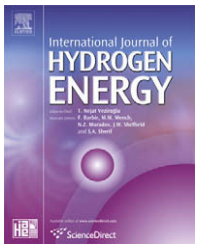

Optimal design of an experimental methanol fuel reformer

Chih-Chiang Chuang[a], Yih-Hang Chen[b], Jeffrey D. Ward[a], Cheng-Ching Yu[a,*], Yen-Chun Liu[c], Chiou-Hwang Lee[c]

[a]Department of Chemical Engineering, National Taiwan University, Taipei 106-07, Taiwan
[b]Energy and Environment Research Laboratories, Industrial Technology Research Institute, Hsinchu 310, Taiwan
[c]Material and Chemical Research Laboratories, Industrial Technology Research Institute, Hsinchu 310, Taiwan

ARTICLE INFO

Article history:
Received 4 July 2008
Received in revised form
19 August 2008
Accepted 19 August 2008
Published online ■

ABSTRACT

We report on the steady state modeling of an experimental methanol fuel reformer for fuel cell applications. The fuel reformer consists of an AutoThermal Reformer (ATR) followed by an Oxygen Removal (OR) reactor, Steam Reformer (SR) and Water Gas Shift (WGS) reactor. The effluent from the WGS is fed to a series of three Preferential Oxidation (PROX) reactors that reduce the CO concentration to less than 40 ppm. A mathematical model of the reformer is developed and selected parameters of the model are fit to experimental data collected from a fuel reformer that was designed, built and operated by the Material and Chemical Research Laboratories (MCL) of the Industrial Technology Research Institute (ITRI) in Hsinchu, Taiwan. In order to develop a compact and high-performance fuel reformer system, the mathematical model is used to design a reformer that has the minimum possible combined volume of the steam reformer and water gas shift reactor. The result is that the volume of the optimized reactor units can be reduced by 17.2% without a significant change in the overall efficiency.

1. Introduction

As a method of power generation, fuel cells have the potential to provide higher efficiency and therefore also reduced emissions compared to internal combustion engines [1]. Fuel cells have been designed that can directly oxidize fuels such as methane, methanol, dimethylether, etc. However, the greatest efficiency is achieved when elemental hydrogen is oxidized directly at the anode. However, as a fuel, hydrogen is difficult to store and transport. Therefore, in recent decades, considerable effort has been made in the design of fuel reforming systems that can produce a hydrogen-rich stream from a fuel such as methanol, ethanol, dimethyl ether or hydrocarbon fuels. A detailed review is given by Song [2]. Further background information is available in Refs. [3,4].

There are a number of considerations in the design of fuel reforming systems [1]. Carbon monoxide is a poison for polymer electrolyte membrane (PEM) fuel cells, thus if this kind of fuel cell is used, the carbon monoxide concentration must be reduced to a very low level, typically less than 100 ppm. For transportation applications in particular but for stationary applications as well, it is desirable to make the fuel reforming system as small and lightweight as possible. Because many fuel reforming reactions take place at high temperatures, it is desirable to employ heat integration in order to improve the efficiency of the reforming process. Finally, it is desirable that the fuel reforming system start up

* Corresponding author.
E-mail address: ccyu@ntu.edu.tw (C.-C. Yu).

0360-3199/$ – see front matter © 2008 International Association for Hydrogen Energy. Published by Elsevier Ltd. All rights reserved.
doi:10.1016/j.ijhydene.2008.08.045

Nomenclature

A	reactor cross-section area (m^2)
$C_{P,g}$	heat capacity of gas (J/(mol K))
$C_{P,S}$	heat capacity of solid (J/(kg K))
F	molar flow rate (mole/min)
h	heat transfer coefficient (J/(min m^2 K))
$\Delta H_{rxn,j}$	reaction heat of jth reaction (J/mol)
k_{cond}	thermal conductivity of solid (J/(min m K))
Q_{loss}	heat loss per unit reactor volume(J/min/m^3)
r_j	jth reaction (mol/kg/min)
S	geometric surface area per unit reactor volume (m^2/m^3)
T_a	temperature of ambient (K)
T_g	temperature of gas (K)
T_S	temperature of solid (K)
U	overall heat transfer coefficient (J/(m^2 min K))
V_n	reactor volume of each lump (m^3)
$W_{cat,n}$	catalyst weight of each lump (kg)
y_i	mole fraction of component i
z	axial direction in a reactor

Greek letters

ρ_{cat}	molar density of catalyst (mol/m^3 of support)
ρ_g	molar density of gas (mol/m^3 of gas)
ρ_S	density of solid (kg/m^3 of support)
ν_{ij}	stoichiometry coefficient of ith component in jth reaction
ε	void fraction of the monolith (m^3/m^3 of reactor volume)

subscripts

i	index of component
j	index of reaction
n	index of lump in the reactor
S	solid
g	gas

and achieve steady state quickly, and respond quickly to changes in hydrogen demand.

Many fuels have been proposed for reforming to produce hydrogen, including methane, methanol, dimethyl ether, ethanol and even gasoline. Among these, methanol has the advantages that it has a relatively high hydrogen-carbon ratio, it is a liquid at room temperature, and it can be formed either from natural gas or from biomass. A number of authors have studied methanol fuel reforming for fuel cell applications, including Refs. [5–15].

In this contribution, we report on the steady-state modeling and design optimization of a 1.5 kW methanol fuel reformer built and operated by the Material and Chemical Research Laboratories (MCL) of the Industrial Technology Research Institute (ITRI) in Hsinchu, Taiwan. The fuel reformer consists of feed preheating unit, autothermal reformer, oxygen removal reactor, steam reformer, high-temperature water gas shift reactor, and preferential oxidation reactors. The experimental set-up and analysis are similar to work previously reported [16] for a methane fuel reformer system.

According to a US Department of Energy report [17], the goals for future PEM fuel cell performance and power generation per volume of a feed reformer are 75%(LHV) and 2 kW/L by 2015. Reducing the volume of fuel reforming systems is an important step toward meeting these goals. Therefore, in this work an optimized design with a minimized fuel reformer volume is also developed.

This manuscript is organized as follows: In Section 2, the experimental setup is described. In Section 3 each reactor unit is discussed, and the mathematical model that is used to describe each unit is given, including the chemical reactions that are assumed to take place and the rate equations that describe them. In Section 4, experimental data from the MCL fuel reformer is given, and the method used to adjust model parameters and the results of the fitting are described. In Section 5, it is shown how the mathematical model was used to design an optimized process that has the minimum possible combined volume of the steam reformer and water gas shift reactor. Finally, in Section 6 conclusions are presented.

2. Experimental

2.1. Experimental set-up

The experimental fuel processor was designed and installed in the facility of MCL of ITRI. The entire fuel processor setup is composed of several reactors, heat exchangers, and a pre-heating system (Regenerative Thermal Oxidizer (RTO)). A process flow diagram for the fuel reformer system is shown in Fig. 1. The feeds enter the system at room temperature. The methanol, water and air feed flow rates can be adjusted by pumps and a blower. The methanol and water mixture first passes through the RTO which uses a catalyst to burn residual hydrogen in the fuel cell exhaust gas or off-spec reformate gas to heat the feed stream and vaporize the water and methanol.

The vapor mixture then passes into the autothermal reformer. The reformer is made of stainless steel 304 with good heat transfer capability. Monolith catalyst carrier is placed inside the reformer and the catalyst is coated on a ceramic support. The catalyst used here is a Pt/CeO_2–ZrO_2 catalyst developed by MCL of ITRI. Adding Pt on the catalyst surface increases the thermal resistance of the catalyst.

The hot reformer effluent is cooled down using a heat exchanger and direct water injection before entering the oxygen removal reactor. The purpose of the oxygen removal reactor is to remove the oxygen from the outlet stream of the autothermal reformer, because oxygen will poison the commercial $Cu–ZnO/Al_2O_3$ (MDC-3) catalyst in the steam reformer.

After passing through the oxygen removal reactor, the reformed fuel gas enters the steam reformer reactor. Following the steam reformer is the water gas shift reactor. Water injection between these two reactors is employed to cool the fuel gas. The operating temperature of the high-temperature water gas shift reactor (HTS) is 310 °C and the

Please cite this article in press as: Chuang C-C et al., Optimal design of an experimental methanol fuel reformer, International Journal of Hydrogen Energy (2008), doi:10.1016/j.ijhydene.2008.08.045

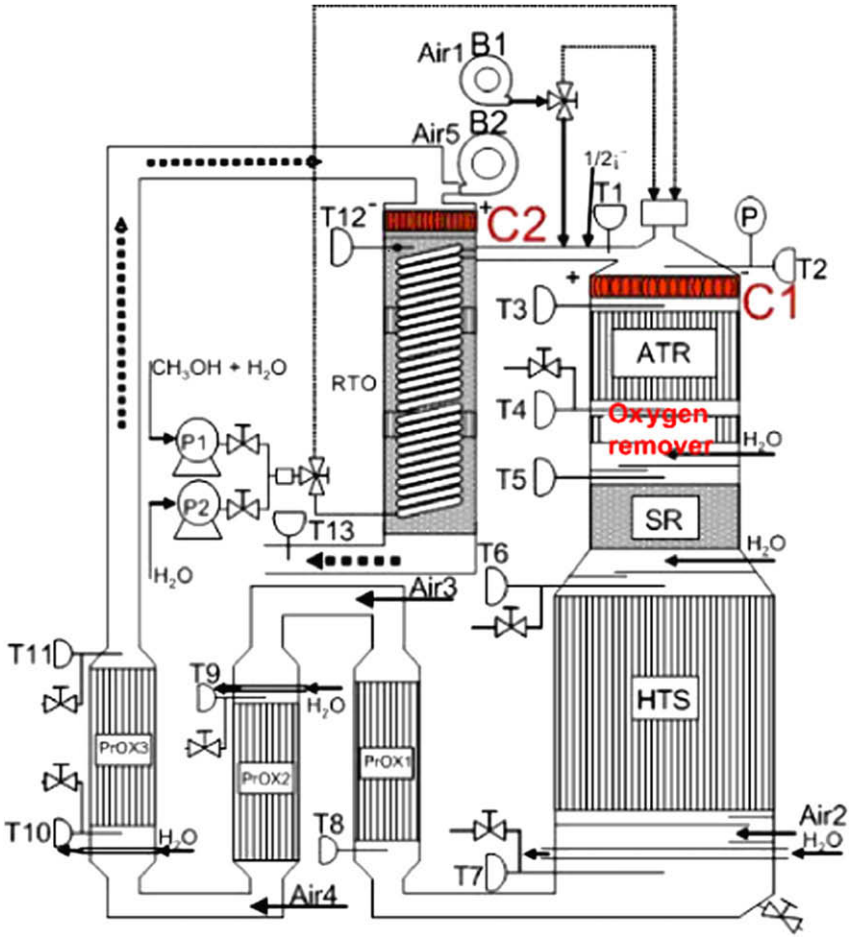

Fig. 1 – Detailed process diagram showing all reactor units, pipes, valves and temperature measurements.

catalyst is a Pt/mixed-oxide catalyst developed by MCL of ITRI and coated on honeycomb catalyst carriers.

The final step in the fuel reforming process is preferential oxidation (PROX). Oxygen is introduced before the fuel gas enters the PROX reactors. A catalyst containing 3 wt% Pt prepared by MCL of ITRI catalyzes the PROX reactions. All dimensions and catalyst properties of all reactors are shown in Tables 1 and 2.

2.2. *Experimental runs and results*

The objectives of this experimental setup are to (1) test the reactivity and properties of the catalysts developed by MCL of ITRI; (2) obtain operating parameters to achieve the desired hydrogen flow rate and carbon monoxide concentration; and (3) collect data to develop a mathematical model of the process.

The experiment is operated in two stages: (1) heat-up and (2) autothermal reforming.

The start-up procedure of the methanol steam reformer is as follows:

Methanol and water are mixed in the pre-mixing tank and pumped into the autothermal reformer. In front of the autothermal reformer, an igniter system is used to preheat the methanol and water by using nickel–chromium filament. The igniter system starts to heat the nickel–chromium filament in the first 3 min. Then, methanol solution and air (oxygen) are fed into the autothermal reformer to carry out the combustion reaction. A large quantity of fuel is consumed to heat up the catalyst and monolith support of the reformer. During startup, the reformate gas is sent to the RTO unit and combusted to release energy. When the temperature of RTO is satisfactory, the igniter system is turned off. The RTO instead of igniter becomes the feed preheating unit. When the concentration of CO in outlet stream of the PROX reactor reaches the ppm level, the reformate gas is fed into PEM Fuel cell system. Figs. 2 and 3 show the results of typical experimental runs, including both startup and steady-state reforming operation. Fig. 2 shows the temperatures profiles for different sectors of the fuel processor. Fig. 3 gives the concentration profiles for CO and hydrogen.

Table 1 – Reactor dimensions

	ATR	Oxygen remover	SR	HTS	PROX1	PROX2	PROX3
Height (cm)	4	1	3	10	9	9	9
Outer diameter (cm)	8	8	8	11.8	7.6	7.6	7.6

Please cite this article in press as: Chuang C-C et al., Optimal design of an experimental methanol fuel reformer, International Journal of Hydrogen Energy (2008), doi:10.1016/j.ijhydene.2008.08.045

Table 2 – Catalyst properties

	ATR	Oxygen remover	SR	HTS	PROX1	PROX2	PROX3
Type of support	Ceramic monolith 400 cell/in^2	Ceramic monolith 400 cell/in^2	Tablet ψ6.4 × 3.2 mm	Ceramic monolith 400 cell/in^2	Metal monolith 300 cell/in^2	Metal monolith 300 cell/in^2	Metal monolith 300 cell/in^2
Volume of support (ml)	201.1	50.3	151.2	1093.6	364.7	364.7	364.7
Catalyst weight (g)	39.0	16.5	204.6	186.5	74.4	70.4	68.8

3. Reactor models

A process flow diagram for the fuel reformer system is shown in Fig. 1. All reactor units are modeled as plug flow reactors (PFRs). At steady state, the models consist of coupled nonlinear ordinary differential equations that describe the change in gas phase molar flow rate and reactor temperature down the length of the reactor. All units except the ATR are well insulated; therefore, it is assumed that they are adiabatic. It is further assumed that the ideal gas equation of state is valid, and that the pressure drop across the reactor units is negligible. For the gas phase flow rates, a material balance on each species gives:

$$\frac{1}{A}\frac{dF_i}{dz} = (1-\varepsilon)\sum_j \nu_{ij} r_j \rho_{cat} \quad (1)$$

where A, F, ν, ε, r and ρ_{cat} are the reactor cross-sectional area, species molar flow rate, stoichiometry coefficient, void fraction, reaction rate and catalyst density, respectively. The subscripts i and j refer to species and reactions, respectively. For the temperature of the gas in the reactor:

$$\frac{1}{A}\frac{d}{dz}\left(\sum_i F_i C_{P,i} T_g\right) = hS(T_S - T_g) \quad (2)$$

where h is the heat transfer coefficient between the catalyst surface and the gas phase, S is a geometric factor equal to the catalyst surface area per unit catalyst volume, and T_S and T_g are the temperature of the catalyst surface and the gas in the reactor, respectively.

For the temperature of the solid catalyst:

$$-\frac{k_{cond}}{A}\frac{d^2T_S}{dz^2} = (1-\varepsilon)\sum_j (-\Delta H_{rxn,j}) r_j \rho_{cat} - hS(T_S - T_g) - Q_{loss} \quad (3)$$

Q_{loss} is a term that accounts for loss of thermal energy to the environment. Q_{loss} is assumed to be negligible for every unit except the ATR, that is all units except the ATR are well insulated and therefore assumed to be adiabatic. For the ATR, Q_{loss} is calculated according to:

$$Q_{loss} = \frac{4U}{D}(T_S - T_a) \quad (4)$$

where U is the overall heat transfer coefficient and D is the outside diameter of the ATR.

Eqs. (1)–(3) apply to every reactor in the fuel processor; however, a different set of reactions are assumed to take place in each reactor. Table 3 summarizes the reactions that take place in each reactor, together with the enthalpy of the reaction, the kinetic expression used, and the literature reference for the kinetic expression.

In the autothermal reactor three reactions may take place: methanol is reversibly converted to carbon monoxide and hydrogen, carbon monoxide and water can convert reversibly to carbon dioxide and hydrogen (the water gas shift reaction), and methanol can be oxidized to form carbon dioxide and water. In the steam reforming reactor, only the water gas shift reaction and the reversible conversion of methanol to carbon monoxide and hydrogen can occur. In the WGS reactor only the WGS reaction can occur. Finally, in the PROX reactor, carbon monoxide is catalytically oxidized to form carbon dioxide, and some hydrogen is oxidized as well. Tables 4–6 summarize the literature values of the kinetic and absorption parameters for the reactions.

Cooling between reactor units is accomplished either by heat exchange with cooling water or direct cold water injection. Where direct injection of water was employed, the

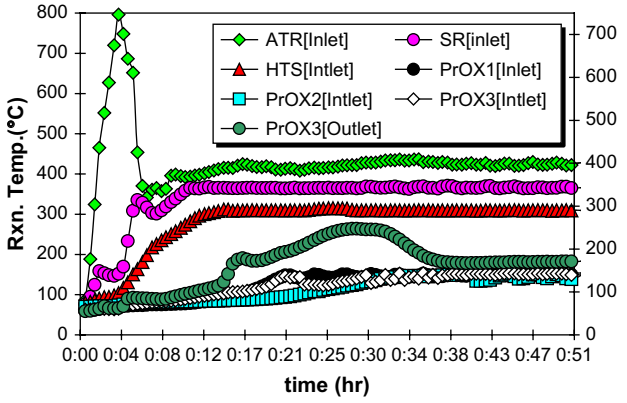

Fig. 2 – Temperature versus time at various points in the fuel reformer system.

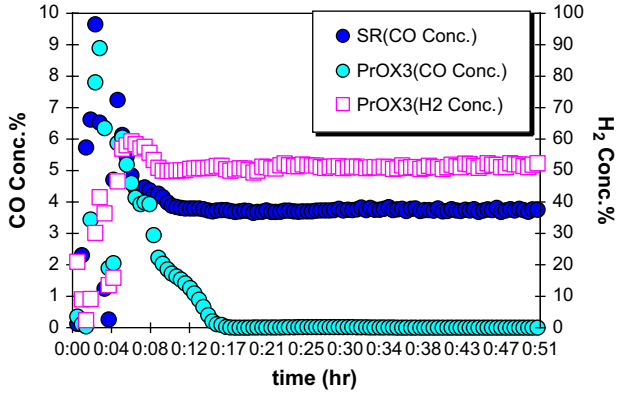

Fig. 3 – Concentration versus time at various points in the fuel reformer system.

Please cite this article in press as: Chuang C-C et al., Optimal design of an experimental methanol fuel reformer, International Journal of Hydrogen Energy (2008), doi:10.1016/j.ijhydene.2008.08.045

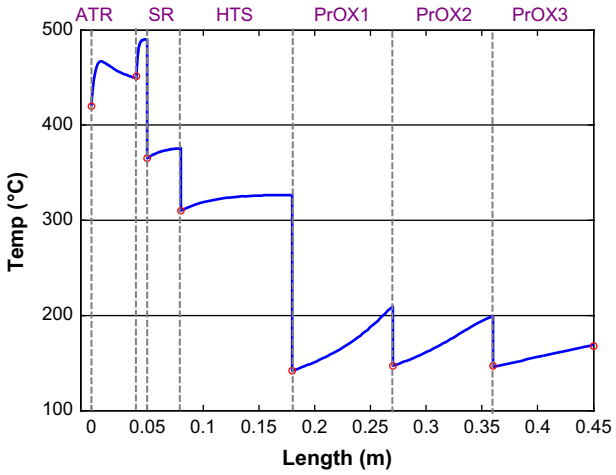

Fig. 4 – Temperature profile indicated by the mathematical model (solid line) and experimental data (open circles).

following energy balance is used to calculate the outlet temperature:

$$\sum_i F_{i,out}\int_{T_{out}}^{T_{in}} C_{P,i}\,dT = -F_{H_2O,in}\times\left(C_{P,H_2O(l)}(373-298)+\Delta H_{H_2O}^{vap}+\int_{T_{373}}^{T_{in}} C_{P,H_2O(g)}(T)\,dT\right) \quad (5)$$

where the term on the left hand side represents the temperature change of the hydrogen-rich gas stream and the right hand side represents the temperature increase and vaporization of the injected water.

4. Experimental data and parameter fitting

The fuel reformer was operated at steady state with the feed conditions given in Table 7. The temperature and composition of the gas stream exiting each reactor was measured. Table 8 shows the steady-state inlet and outlet temperature and outlet composition for each reactor unit. In order to match the experimental data to the mathematical model, certain model parameters were adjusted iteratively according to the following procedure:

(1) Initial values are supplied for the parameters U and k_{cond} and the parameter group (hS).
(2) Adjust certain kinetic parameters in order to match the steady-state reactor effluent compositions as closely as possible.
(3) Using the values of the kinetic parameters from (2), calculate the temperature at the reactor effluent and compare with the experimental results. If there is significant deviation, return to (1) and adjust the parameters U and k_{cond} and the parameter group (hS). If there is no significant deviation, proceed to (4).
(4) Adjust capacity parameters $\varepsilon\rho_g$, $\varepsilon\rho_g C_{p,s}$,$(1-\varepsilon)\rho_s C_{p,s}$ in order to match the dynamic response of the process. If a match is possible, then the process parameters have been appropriately identified. If not, return to (1) and adjust U and k_{cond} and the parameter group (hS).

Table 9 shows the values of the physical property parameters that were identified by this procedure. Tables 10 and 11 show the modified kinetic parameters, together with their literature values.

Although this paper discusses only a steady-state process model, in step (4) some of the parameters of the steady-state

Table 3 – Reactions and kinetics

Reaction	ΔH_{298} kJ/mol	Kinetics	Reference	Note
Autothermal reactor (ATR)				
$CH_3OH \rightleftarrows CO + 2H_2$	90.5	$r_{MD} = \frac{K_{a,2}(k_D P_{CH_3OH} - k_{D,B} P_{H_2}^2 P_{CO}) C_{S2} C_{S2a} S_g}{(P_{H_2}^{0.5} + K_{a,2} P_{CH_3OH} + K_{b,2} P_{H_2O})(1 + K_{c,2}^{0.5} P_{H_2}^{0.5})}$	[5–7]	
$CO + H_2O \rightleftarrows CO_2 + H_2$	−41.2	$r_W = \frac{K_{b,1}(k_W P_{CO} P_{H_2O} - k_{W,B} P_{H_2} P_{CO_2}) C_{S1}^2 S_g}{(P_{H_2}^{0.5} + K_{a,1} P_{CH_3OH} + K_d P_{CO_2} P_{H_2} + K_{b,1} P_{H_2O})^2}$	[5–7]	
$CH_3OH + 1.5O_2 \rightarrow CO_2 + 2H_2O$	−675.4	$r_{OX} = k_{OX} P_{CH_3OH} P_{O_2}^{1.5}$	–	a
Oxygen removal reactor (OR)				
$CH_3OH + 1.5O_2 \rightarrow CO_2 + 2H_2O$	−675.4	$r_{OX} = k_{OX} P_{CH_3OH} P_{O_2}^{1.5}$	–	a
Steam reforming reactor (SR)				
$CH_3OH \rightleftarrows CO + 2H_2$	90.5	$r_{MD} = \frac{K_{a,2}(k_D P_{CH_3OH} - k_{D,B} P_{H_2}^2 P_{CO}) C_{S2} C_{S2a} S_g}{(P_{H_2}^{0.5} + K_{a,2} P_{CH_3OH} + K_{b,2} P_{H_2O})(1 + K_{c,2}^{0.5} P_{H_2}^{0.5})}$	[5–7]	
$CO + H_2O \rightleftarrows CO_2 + H_2$	−41.2	$r_W = \frac{K_{b,1}(k_W P_{CO} P_{H_2O} - k_{W,B} P_{H_2} P_{CO_2}) C_{S1}^2 S_g}{(P_{H_2}^{0.5} + K_{a,1} P_{CH_3OH} + K_d P_{CO_2} P_{H_2} + K_{b,1} P_{H_2O})^2}$	[5–7]	
Water gas shift (HTS)				
$CO + H_2O \rightleftarrows CO_2 + H_2$	−41.2	$r_{WGS} = k_{WGS}(P_{CO} P_{H_2O} - \frac{P_{CO_2} P_{H_2}}{K_{WGS}})$	[18]	
Preferential Oxidation (PROX)				
$CO + \frac{1}{2}O_2 \rightarrow CO_2$	−283	$r_{CO} = \frac{k_{CO} P_{CO} P_{O_2}}{(1 + K_{CO} P_{CO})^2}$	[19]	
$H_2 + \frac{1}{2}O_2 \rightarrow H_2O$	−242	$r_{H_2} = k_{H_2} P_{H_2}^{0.5}$	[20]	b

a The form of the kinetic rate expression for methanol oxidation was developed by assuming a quasi-elemental reaction. The activation energy for the reaction is taken from the literature [11]. The pre-exponential factor was determined by regression of experimental data.
b The form of this kinetic rate expression is modified from [20].

Please cite this article in press as: Chuang C-C et al., Optimal design of an experimental methanol fuel reformer, International Journal of Hydrogen Energy (2008), doi:10.1016/j.ijhydene.2008.08.045

Table 4 – Literature values of kinetic parameters for the autothermal reactor (ATR), steam reforming reactor, and oxygen removal reactor

Kinetic parameter	Pre-exponential factor a_0 (rate constant)	Activation energy E_A (kJ/mol)
k_D	2.28×10^{22} mol/(g min bar)	170
$k_{D,B}$	8.57×10^{10} mol/(g min bar^2)	80
k_W	3.54×10^{15} mol/(g min bar)	87.6
$k_{W,B}$	5.42×10^{17} mol/(g min bar)	128.8
k_{OX}	–	115

model were determined by matching the dynamic response of the process with a dynamic model. Appendix A gives additional details about the procedure that was used. If a satisfactory match between the calculated and experimentally determined trajectories was not achieved, then the numerical values of the physical property parameters were again adjusted and the procedure repeated. Table 12 shows the values of the capacity parameters that were identified using dynamic data.

Figs. 4–6 show the steady state temperature and composition profiles in the reactor as suggested by the mathematical model, along with the experimental data points. Fig. 4 shows the temperature profile, Fig. 5 shows the mole fraction of methanol (left axis) and oxygen (right axis) on logarithmic scales, and Fig. 6 shows the composition of CO_2 and H_2 (left axis, linear scale) and CO (right axis, logarithmic scale). Along the top of each figure are labels that identify each reactor in the process. Note that as shown in Fig. 1 there is water injection after the oxygen removal and steam reforming reactors, and inter-stage cooling and oxygen injection before each of the PROX reactors.

In the autothermal reactor, the temperature rises rapidly as the highly exothermic oxidation reaction (R_{OX}) occurs first, and then decreases as the endothermic molecular decomposition reaction (R_{MD}) and reverse water gas shift reaction (R_W) proceed. Some thermal energy is also lost to the environment. In the ATR, the concentration of methanol and oxygen drop rapidly (Fig. 5), while the concentration of CO_2, H_2 and CO rapidly rise (Fig. 6), consistent with the occurrence of all three reactions.

In the oxygen removal reactor, the temperature rises due to the highly exothermal oxidation reaction (Fig. 4), while the concentration of oxygen rapidly drops almost to zero (Fig. 5). This is necessary because any oxygen present at this point in the gas stream will poison the copper catalyst in the water gas shift reactor.

In the steam reforming and water gas shift reactors, the temperature rises gradually (Fig. 4) due to the exothermic WGS reaction. The concentrations of hydrogen and carbon dioxide gradually rise, while the concentration of CO gradually falls, which is also consistent with the occurrence of the water gas shift reaction (Figs. 5,6).

Before each of the PROX reactors, the gas stream is cooled in a heat exchanger and oxygen is injected into the reactor. The temperature rises in the reactor because the oxidation reactions are exothermic. Because concentrations are expressed on a mole fraction basis, there are discontinuities in the mole fraction of all species when air is injected into the system, because the air injection increases the total number of moles of gas in the stream. In each PROX reactor, the concentration of CO decreases and the concentration of CO_2 increases, while there is a very slight decrease in the hydrogen concentration.

Table 5 – Literature values of adsorption parameters for the autothermal reactor (ATR), steam reforming reactor, and oxygen removal reactor

Parameter	Pre-exponential factor A_0 (adsorption constant)	Adsorption ΔH^0 (kJ/mol)
$K_{a,1}$	6.65×10^{-3} bar$^{-0.5}$	−20
$K_{a,2}$	3.69×10^{1} bar$^{-0.5}$	−20
$K_{b,1}$	4.74×10^{-3} bar$^{-0.5}$	−20
$K_{b,2}$	3.69×10^{1} bar$^{-0.5}$	−20
K_c	5.43×10^{-6} bar$^{-0.5}$	−50
K_d	2.3×10^{9} bar^{-2}	100

Table 6 – Literature values of kinetic parameters for the WGS and PROX reactors

Reaction	Pre-exponential factor A_0 (rate constant)	Activation energy E_A (KJ/mol)
k_{WGS}	4.933×10^{6} mol/(g min bar^2)	47.4
k_{WGS}	1.312×10^{-2} (dimensionless)	−38.06
k_{CO}	2.15×10^{16} mol/(g min bar^2)	75.41
K_{CO}	1.248×10^{3} bar^{-1}	3.13
k_{H_2}	1.232×10^{3} mol/(g min bar$^{-0.5}$)	18.74

5. Design optimization

5.1. *Optimization of the fuel reformer volume*

One key consideration in the design of fuel reformers, particularly for transportation applications, is the weight and volume of the reformer components. Therefore, after a mathematical model of the process was developed, a design optimization was conducted, with the objective of minimizing the combined volume of the fuel reformer reactor units. Table 2 shows the volume of each reactor unit. The largest contributions to the total volume come from the HTS and PROX reactors (48% and 42% of the total volume, respectively). Our experience indicates that it is difficult to reduce PROX reactor

Table 7 – Steady state values of feed flow rates into the ATR

Feed CH_3OH (mol/min)	Feed H_2O (mol/min)	Feed O_2 (mol/min)
0.575	0.92	0.115

Please cite this article in press as: Chuang C-C et al., Optimal design of an experimental methanol fuel reformer, International Journal of Hydrogen Energy (2008), doi:10.1016/j.ijhydene.2008.08.045

Table 8 – Steady state composition data

	CO% (dry base)	CO_2% (dry base)	H_2% (dry base)	CH_3OH Conv (%) (dry base)	O_2 Conv (%)	T_{in} (°C)	T_{out} (°C)
ATR	6.2	17.04	53.64	94	90	423	451
Pt/Cz75R	–	–	–	–	100	–	–
SR	3.87	18.8	55.22	–	–	365	–
HTS	1.01	20.88	56.44	–	–	310	143
PROX3	37 (ppm)	20.91	51.59	–	–	143	170

Table 9 – Physical property parameters

Parameter	Value	Units
K_{cond}	1.0	J/(m min K)
U	200	J/(min m^2 K)
hS	1.5×10^5	J/(min m^3 K)

Table 10 – Modified kinetic parameters for the ATR

Pre-exponential factor (rate constant)	Literature	Modified
k_D mol/(g min)	2.28×10^{22}	1.37×10^{18}
k_W mol/(g min bar)	3.54×10^{15}	1.18×10^{19}
$k_{W,B}$ mol/(g min bar)	5.42×10^{17}	5.42×10^{16}
k_{OX} mol/(g min $bar^{2.5}$)	–	6.83×10^{-6}

Table 11 – Modified kinetic parameters for the SR, WGS and PROX reactors

Pre-exponential factor (rate constant)	Literature	Modified
SR: k_D mol/(g min)	2.28×10^{22}	2.3×10^{19}
SRk_W mol/(g min bar)	3.54×10^{15}	2.61×10^{15}
HTSk_{WGS} mol/(g min bar^2)	4.933×10^6	3.09×10^6
PROXk_{CO} mol/(g min bar^2)	2.15×10^{16}	1.89×10^{16}
PROXk_{H_2} mol/(g min $bar^{0.5}$)	1.232×10^3	6.16×10^4

Table 12 – Mass and energy capacity parameters

Parameter	Value	Units
ε	0.8928	
ρ_g	300.0	mol/m^3
ρ_S	1550	mol/m^3
$C_{P,g}$	30	J/(mol K)
$C_{P,S}$	1000	J/(mol K)

volume without violating the CO constraint; however, it is possible to reduce the volume of the HTS reactor.

Because the SR and HTS reactors work together to reduce the CO concentration in the ATR outlet, we attempted to find

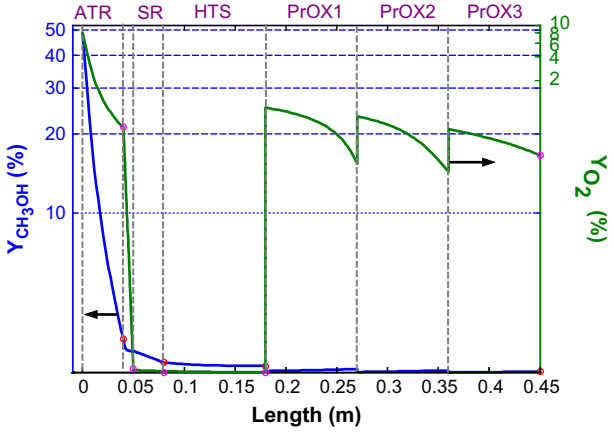

Fig. 5 – Composition profile for methanol and oxygen in the fuel reformer system. Solid lines represent the mathematical model, and open circles represent experimental data.

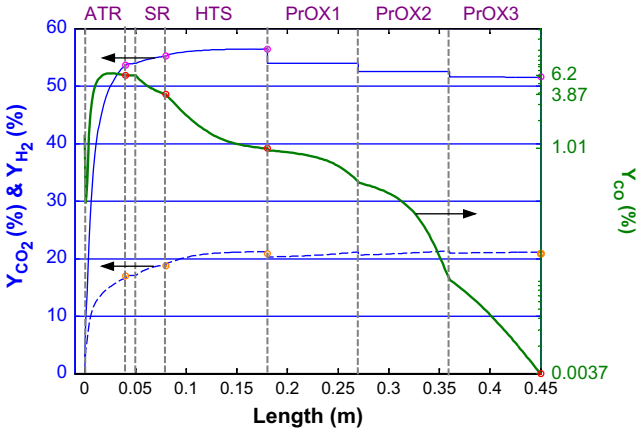

Fig. 6 – Composition profile for hydrogen, carbon dioxide, and carbon monoxide in the fuel reformer system. Lines represent the mathematical model, and open circles represent experimental data. For CO_2 and H_2 concentrations, which are read on the left axis, the solid line represents H_2 concentration and the dashed line represents CO_2 concentration.

Please cite this article in press as: Chuang C-C et al., Optimal design of an experimental methanol fuel reformer, International Journal of Hydrogen Energy (2008), doi:10.1016/j.ijhydene.2008.08.045

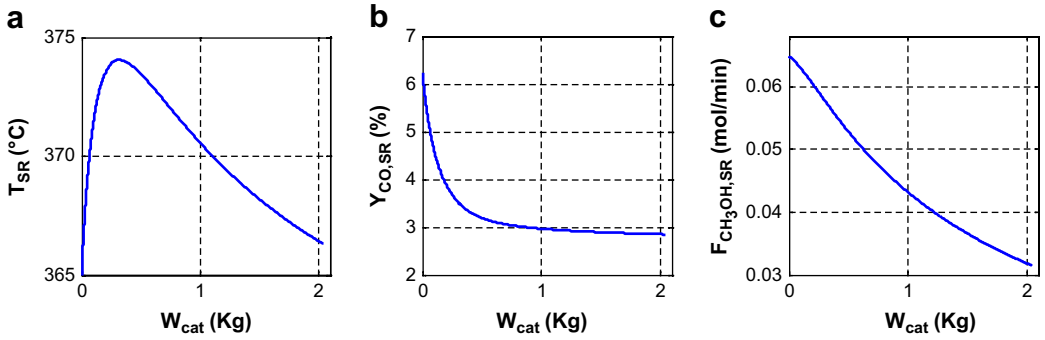

Fig. 7 – Steam reformer properties versus catalyst mass (a) Temperature, (b) CO mole fraction, and (c) methanol flow rate.

the design that minimized the combined volume of these two units, subject to certain constraints. The independent variables for the optimization were the inlet temperature to those reactor units. Note that the volumes of the SR and HTS can be adjusted independently in the optimization.

The objective can be stated mathematically as:

$$\text{Minimize}: f(\mathbf{X}) = (V_{SR} + V_{HTS}) \tag{6}$$

$$\mathbf{X} = \{T_{SR,in}, T_{HTS,in}\} \tag{7}$$

$$\text{Subject to}: \begin{Bmatrix} T_{SR,out} - T_{HTS,in} \geq 10^{\circ}C \\ \frac{dT_{SR,out}}{dW_{cat}} = 0 \\ T_{HTS,out} < 350^{\circ}C \\ Y_{CO,HTS} = 1.01\% \end{Bmatrix} \tag{8}$$

It is worthwhile to discuss the implications of the constraints given in Eq. (8) and the reasons that they are included in the optimization. The first constraint specifies a minimum difference in the temperature between the SR outlet and the HTS inlet. The difference is necessary to allow for proper automatic temperature control (by water injection). The third constraint is a maximum reactor temperature constraint due to the properties of the HTS Cu–ZnO/Al_2O_3 catalyst. The fourth constraint specifies the maximum allowable CO concentration at the HTS outlet. When the CO concentration at the exit of the HTS is below this level, it can be reduced to the PPM level by the PROX reactors.

The second constraint is not as intuitive as the others, but it is necessary in order to ensure that the optimization produces a reasonable process design. The reason for including the second constraint can be understood in light of Fig. 7, which shows several steam reformer properties plotted versus catalyst mass (i.e. position in the plug flow reactor). The methanol concentration (Fig 7(c)), which is already low, drops continuously throughout the reactor because of the methanol decomposition reaction. The reactor temperature (Fig 7(a)) rises at first because the exothermic water gas shift reaction dominates, consuming carbon monoxide (Fig 7(b)). Farther down the reactor, this reaction becomes less

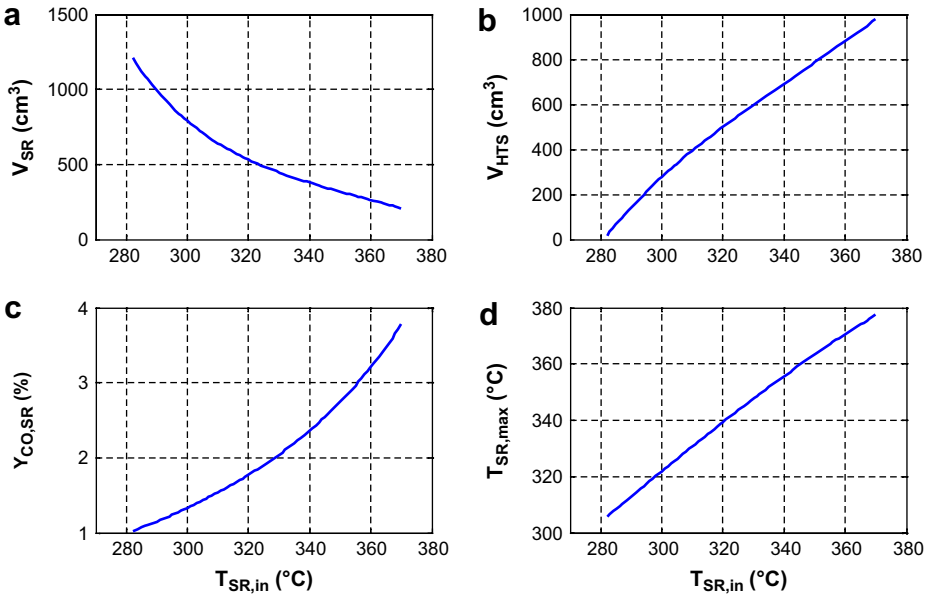

Fig. 8 – System properties as a function of steam reformer inlet temperature calculated using process model. (a) SR volume, (b) HTS volume, (c) mole fraction of CO in SR outlet, and (d) maximum temperature in SR.

Please cite this article in press as: Chuang C-C et al., Optimal design of an experimental methanol fuel reformer, International Journal of Hydrogen Energy (2008), doi:10.1016/j.ijhydene.2008.08.045

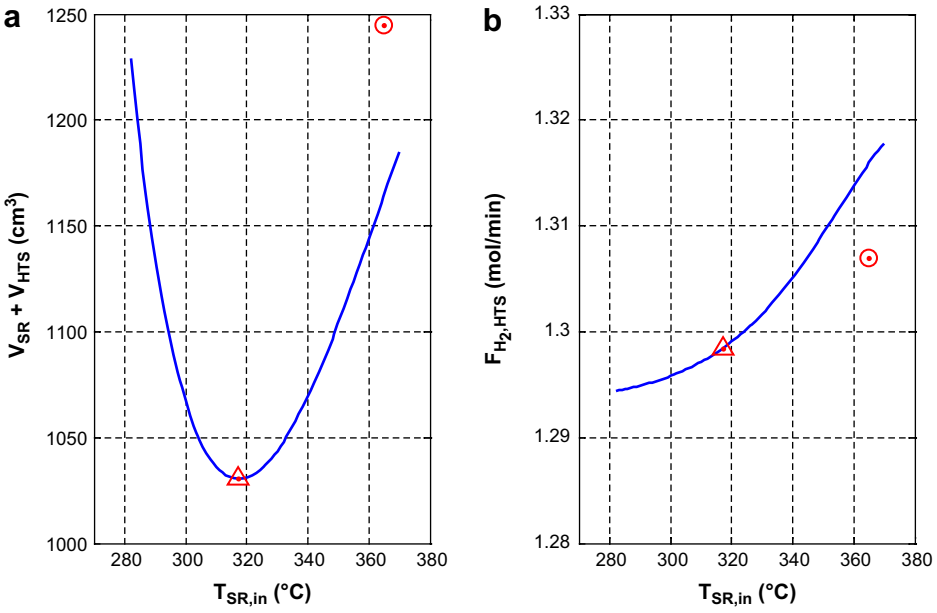

Fig. 9 – Combined volume of the steam reforming reactor and the HTS reactor (a) and HTS outlet hydrogen flow rate (b) versus steam reformer inlet temperature.

important and the endothermic methanol decomposition reaction, which produces carbon monoxide, becomes more important. As a result, the concentration of carbon monoxide in the steam reformer drops quickly initially but then plateaus. A practical design will include a steam reformer sized so that the CO concentration is beginning to plateau at the exit of the reactor. This outcome can be guaranteed by requiring that the derivative of reactor temperature with respect to catalyst mass at the exit of the reactor be equal to zero.

The optimization problem was solved by iterating over the two optimization variables. For a given value of $T_{SR,in}$, the value of $T_{HTS,in}$ that minimized the combined volume was identified. The procedure was repeated for various values of $T_{SR,in}$ until the global minimum was identified.

Fig. 8 shows certain properties of the fuel reformer system versus $T_{SR,in}$ with the optimal (volume-minimizing) value of $T_{HTS,in}$. As the SR inlet temperature increases, the SR volume decreases (Fig 8(a)). The maximum temperature of the SR also increases with increasing inlet temperature (Fig 8(d)). The higher temperature is favorable from a kinetic point of view and the WGS reaction approaches equilibrium more quickly in this case. However, the higher temperature is also disadvantageous from a thermodynamic point of view: the equilibrium CO concentration is greater at higher temperatures (Fig 8(c)). As a result, the mole fraction of CO at the SR outlet increases with increasing temperature, as does the required volume of the HTS (Fig 8(b)). The higher SR reactor temperature will cause a higher CO concentration in the SR outlet stream. This means that a larger HTS reactor volume will be needed to meet the CO concentration specifications in the HTS outlet stream. Therefore, there is a tradeoff in the reactor network design and a minimum in the combined reactor volume.

Fig. 9(a) shows the combined volume of the steam reformer and HTS reactor versus the inlet temperature of the steam

Table 13 – Reaction and kinetics for methanation reactor

Reaction	Kinetics	Source
$CH_4 + H_2O \rightleftarrows CO + 3H_2$	$r_M = \frac{k_f P_{CH_4} P_{H_2O} - k_r P_{CO} P_{H_2}^3}{P_{H_2}^{2.5}(\alpha)^2}$ $\alpha = \left(1 + K_{CO}P_{CO} + K_{H_2}P_{H_2} + K_{CH_4}P_{CH_4} + K_{H_2O}\frac{P_{H_2O}}{P_{H_2}}\right)$	[21]

Table 14 – Literature values of kinetic parameters for the methanation reaction

Component	Pre-exponential factor A_0 (adsorption constant)	Adsorption ΔH^0(KJ/mol)
k_f mol/(min bar$^{0.5}$)	7.02×10^{16}	240.1
k_r mol/(min bar$^{1.5}$)	5.862×10^{3}	67.1
CH_4 (bar^{-1})	6.65×10^{-4}	−38.3
CO (bar^{-1})	8.23×10^{-5}	−70.7
H_2 (bar^{-1})	6.12×10^{-9}	−82.9
H_2O (bar^{-1})	1.77×10^{5}	88.7

Table 15 – Modified values of kinetic parameters for the methanation reaction

Pre-exponential factor (rate constant)	Literature	Modified
k_f mol/(min bar$^{0.5}$)	7.02×10^{16}	7.02×10^{16}
k_r mol/(min bar$^{1.5}$)	5.862×10^{3}	4.66×10^{4}

Please cite this article in press as: Chuang C-C et al., Optimal design of an experimental methanol fuel reformer, International Journal of Hydrogen Energy (2008), doi:10.1016/j.ijhydene.2008.08.045

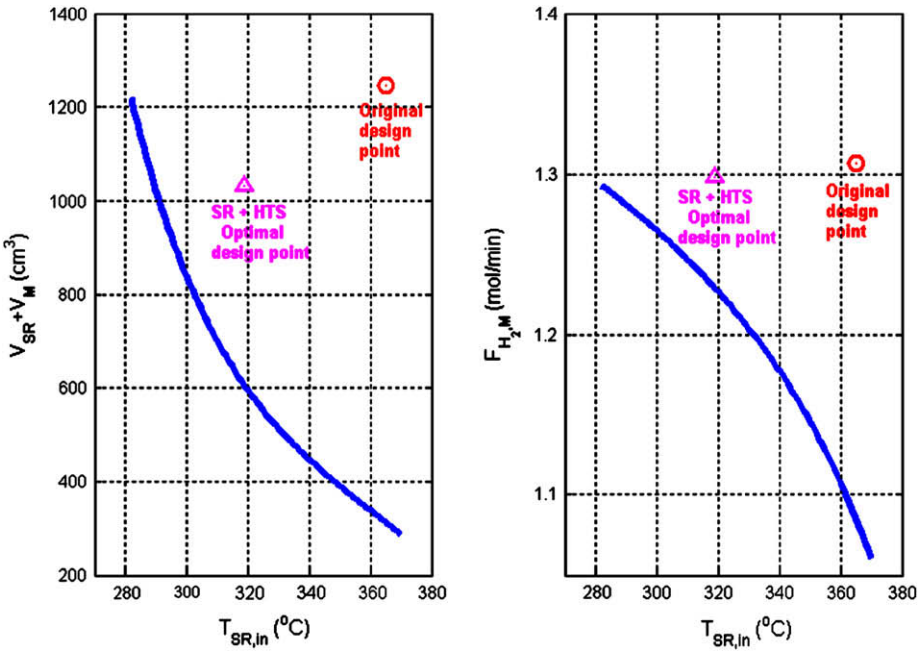

Fig. 10 – Combined volume of the steam reforming reactor and the methanation reactor (a) and HTS outlet hydrogen flow rate (b) versus steam reformer inlet temperature.

reformer. The optimal design is marked with a triangle and the experimental (base case) design is marked with a circle. The minimum combined volume occurs at a temperature of 317 °C and a combined volume of 1031 cm^3, as compared with the initial design at a temperature of 365 °C and 1247 cm^3, for a reduction in volume of 17.2%. The steam reformer inlet temperature in the optimal design is 317 °C.

It is important to verify that the reduction in reformer size does not come at the expense of a significant reduction in the hydrogen production rate (i.e. the efficiency of the reformer). Fig. 9(b) shows the hydrogen flow rate at the exit of the HTS versus the steam reformer inlet temperature. Compared with the base-case design, the hydrogen production rate of the volume-optimized system is reduced by only 0.69%.

5.2. *Optimization of the reaction pathway*

Besides optimizing the process as described above, an alternative way to reduce the fuel reformer volume is to use a different process design in which the HTS reactor is replaced with a methanation reactor. The methanation reactor reduces the CO concentration by hydrogenating CO to form methane and water. Table 13 shows the reaction and the kinetic expression that was used to model the reaction rate [21]. Table 14 shows the literature values of the kinetic parameters taken from [22]. Table 15 shows the modified kinetic parameters that were determined by regressing experimental data for the methanation reaction from MCL of ITRI.

For the alternative process design with the methanation reactor, the optimization problem can be stated as:

$$\text{Minimize}: f(\mathbf{X}) = (V_{SR} + V_M) \tag{9}$$

$$\mathbf{X} = \{T_{SR,in}, T_{M,in}\} \tag{10}$$

$$\text{Subject to}: \begin{Bmatrix} T_{SR,out} - T_{M,in} \geq 10\ ^\circ\text{C} \\ \frac{dT_{SR,out}}{dW_{cat}} = 0 \\ T_{M,out} < 500\ ^\circ\text{C} \\ Y_{CO,HTS} = 1.01\% \end{Bmatrix} \tag{11}$$

Fig. 10(a) shows the combined volume of the steam reforming and methanation reactors versus SR inlet temperature for the optimal value of the methanation inlet temperature. In contrast with Fig. 9(a), the combined volume decreases with increasing temperature over the entire temperature range 280–370 °C. For temperatures beyond 370 °C it is impossible to satisfy the constraints. The minimum possible combined volume is just 287 cm^3, a reduction of 77% compared to the base-case system.

However, from Fig. 10(b) this improvement comes at the expense of a drastic reduction in the hydrogen flow rate. At the design corresponding to the minimum combined volume, the hydrogen flow rate is reduced by 19%. The reason for this is that the methanation reaction consumes three moles of hydrogen for every mole of CO converted. Although the methanation reactor is attractive from the point of view of volume reduction, it results in a prohibitive loss of efficiency of the reformer. Therefore, this process design alternative is not considered any further.

6. Conclusions

In this work, we have reported on the modeling and optimization of an experimental methanol fuel reforming system for

Please cite this article in press as: Chuang C-C et al., Optimal design of an experimental methanol fuel reformer, International Journal of Hydrogen Energy (2008), doi:10.1016/j.ijhydene.2008.08.045

fuel cell applications developed by MCL of ITRI. Kinetic parameters for all of the catalysts, including a Pt/CeO_2–ZrO_2 catalyst developed by MCL of ITRI are identified by fitting experimental data. The experimental system can produce a hydrogen stream with a CO concentration less than 40 ppm, and with an efficiency of 66.1 percent. The method of model development, in which kinetic parameters are taken from the literature and the forward reaction rates are adjusted to match experimental data, has the advantages that it is simple and can be completed rapidly with minimal experimental data, thus facilitating rapid product design.

The model was also used to develop an optimized design in which the volume of the reactor units is minimized. The result of the optimization suggests that the combined volume of the SR and HTS reactors can be reduced by 17.2% with a reduction in the hydrogen flow rate of only 0.69%.

Acknowledgement

This work was supported by the National Science Council of Taiwan under grant NSC 96-2628-E-002-022-MY3.

Appendix A
Determining capacity parameters from dynamic responses

Although this contribution deals only with the development of a steady state model, some of the parameters of the steady state model were estimated by fitting the dynamic response of the process to a dynamic process model. This appendix briefly discusses the development of the dynamic model and the fitting of these parameters.

Eqs. (1)–(3) in the body of the paper are steady-state equations. The analogous dynamic equations are partial differential equations:

$$\varepsilon\rho_g\frac{\partial y_i}{\partial t} = -\frac{1}{A}\frac{\partial(Fy_i)}{\partial z} + (1-\varepsilon)\sum_j \nu_{ij} r_j \rho_{cat} \tag{12}$$

$$\varepsilon\rho_g C_{P,g}\frac{\partial T_g}{\partial t} = -\frac{1}{A}\frac{\partial}{\partial z}\left(\sum_i F C_{P,i} T_g\right) + hS(T_S - T_g) \tag{13}$$

$$\left(1-\varepsilon\right)\rho_S C_{P,S}\frac{\partial T_S}{\partial t} = \frac{k_{cond}}{A}\frac{\partial^2 T_S}{\partial z^2} + (1-\varepsilon)\sum_j\left(-\Delta H_{rxn,j}\right) r_j \rho_{cat} - hS(T_S - T_g) - Q_{loss} \tag{14}$$

These equations are converted into a series of coupled ordinary differential equations by discretizing the length coordinate into a number of finite positions (lumping):

$$\varepsilon\rho_g V_n\frac{dy_{n,i}}{dt} = F_{n-1}y_{n-1,i} - F_n y_{n,i} + \sum_j \nu_{ij} r_{n,j} W_{cat,n} \tag{15}$$

$$\varepsilon\rho_g V_n C_{P,g}\frac{dT_{g,n}}{dt} = F_{n-1}\sum_i y_{n-1,i} C_{P,n-1,i} T_{g,n-1} - F_n \sum_i y_{n,i} C_{P,n,i} T_{g,n} + hSV_n(T_{s,n} - T_{g,n}) \tag{16}$$

$$\left(1-\varepsilon\right)\rho_S V_n C_{P,S}\frac{dT_{S,n}}{dt} = \frac{k_{cond}}{\Delta z^2}(T_{S,n+1} - 2T_{S,n} + T_{S,n-1}) - hSV_n(T_{S,n} - T_{g,n}) + \sum_j\left(-\Delta H_{rxn,j}\right) r_{n,j} W_{cat,n} - Q_{loss} \tag{17}$$

The parameters $\varepsilon\rho_g$, $\varepsilon\rho_g C_{p,s}$, and $(1-\varepsilon)\rho_s C_{p,s}$ were adjusted so that the dynamic trajectories predicted by the model equations match the experimental data. The results are shown in Table 12.

REFERENCES

[1] Ahmed S, Krumpelt M. Hydrogen from hydrocarbon fuels for fuel cells. International Journal of Hydrogen Energy 2001;26:291–301.
[2] Song C. Fuel processing for low-temperature and high-temperature fuel cells: challenges, and opportunities for sustainable development in the 21st century. Catalysis Today 2002;77:17–49.
[3] Larminie J, Dicks A. Fuel cell systems explained. 2nd ed. New York: John Wiley & Sons; 2003.
[4] Fuel cell handbook. 6th ed. EG&G Services Parsons, Inc. Science Applications International Corporation. Morgantown, WV: US Dept. of Energy, 2000.
[5] Asprey SP, Wojciechowski BW, Pepply BA. Kinetic studies using temperature scanning: the steam-reforming of methanol. Appl Catal A Gen 1999;179:51–70.
[6] Pepply BA, Amphlett JC, Kearns LM, Mann RF. Methanol–steam reforming on $Cu/ZnO/Al_2O_3$. Part 1: The reaction network. Appl Catal A Gen 1999;179:21–9.
[7] Pepply BA, Amphlett JC, Kearns LM, Mann RF. Methanol–steam reforming on $Cu/ZnO/Al_2O_3$ catalysts. Part 2. A comprehensive kinetic model. Appl Catal A Gen 1999;179:31–49.
[8] Chan SH, Wang HM. Thermodynamic and kinetic modeling of an autothermal methanol reformer. J Power Sources 2004;126:8–15.
[9] Idem RO, Bakhshi NN. Kinetic modeling of the production of hydrogen from the methanol-steam reforming process over Mn-promoted coprecipitated Cu–Al catalyst. Chem Eng Sci 1996;51(14):3697–708.
[10] Lattner JR, Harold MP. Autothermal reforming of methanol: experiments and modeling. Catalysis Today 2007;120:78–89.
[11] Lattner JR, Harold MP. Compariosn of methanol-based fuel processors for PEM fuel cell systems. Appl Catal B Environ 2005;56:149–69.
[12] Lindstrom B, Pettersson LJ. Hydrogen generation by steam reforming of methanol over copper-based catalysts for fuel cell applications. Int J Hydrogen Energy 2001;26:923–33.
[13] Bichon P, Asheim A, Jordal A, Sperle T, Fathi M, Holmen A, et al. Hydrogen from methanol steam-reforming over Cu-based catalysts with and without Pd promotion. Int J Hydrogen Energy 2007;32:1799–805.
[14] Lee JK, Ko JB, Kim DH. Methanol steam reforming over $cu/Zn/Al_2O_3$ catalyst: kinetics and effectiveness factor. Appl Catal A Gen 2004;278:25–35.

Please cite this article in press as: Chuang C-C et al., Optimal design of an experimental methanol fuel reformer, International Journal of Hydrogen Energy (2008), doi:10.1016/j.ijhydene.2008.08.045

[15] Reitz TL, Ahmed S, Krumpelt M, Kumar R, Kung HH. Characterization of CuO/ZnO under oxidizing conditions for the oxidative methanol reforming reaction. J Mol Catal A Chem 2000;162:275–85.
[16] Lin ST, Chen YH, Yu CC, Liu YC, Lee CH. Modeling of an experimental methane fuel processor. J Power Sources 2005; 148:43–53.
[17] Multi-Year Research, Development and Demonstration Plan: Planned Program Activities for 2005-2015, http://www1.eere.energy.gov/hydrogenandfuelcells/mypp/index.html. accessed 5.30.2008.
[18] Choi Y, Stenger HG. Water gas shift reaction kinetics and reactor modeling for fuel cell grade hydrogen. J Power Sources 2003;124:432–9.
[19] Venderbosch RH, Prins W, van Swaaij WPM. Platinum catalyzed oxidation of carbon monoxide as a model reaction in mass transfer measurements. Chem Eng Sci 1998;53(19): 3355–66.
[20] Choi Y, Stenger HG. Kinetics, simulation and insights for CO selective oxidation in fuel cell applications. J Power Sources 2004;129:246–54.
[21] Xu J, Froment GF. Methane steam reforming, methanation and water-gas shift. I. Intrinsic kinetics. AIChE J 1989;35(1):88–96.
[22] de Smet CRR, de Croon MHJM, Berger RJ, Marin GB, Schouten JC. Design of adiabatic fixed-bed reactors for the partial oxidation of methane to synthesis gas. Application to production of methanol and hydrogen-for-fuel-cells. Chem Eng Sci 2001;56:4849–61.

Please cite this article in press as: Chuang C-C et al., Optimal design of an experimental methanol fuel reformer, International Journal of Hydrogen Energy (2008), doi:10.1016/j.ijhydene.2008.08.045